Proceedings of the Sixth International Conference on
Railway Technology: Research, Development and Maintenance
Edited by: J. Pombo
Civil-Comp Conferences, Volume 7, Paper 20.3
Civil-Comp Press, Edinburgh, United Kingdom, 2024
ISSN: 2753-3239, doi: 10.4203/ccc.7.20.3

Assessing the Impact of Thermal Loading from Brake Shoes on Microstructure and Mechanical Properties in Various Railway Wheel Steels: A Comparative Study

L. Ghidini, A. Mazzu and M. Faccoli

**Department of Mechanical and Industrial Engineering,
University of Brescia
Brescia, Italy**

Abstract

This research delves into the intricate relationship between microstructure and mechanical properties of railway wheels, focusing on the effects of thermal loading induced by brake shoes. Eight distinct wheel steels were investigated, revealing significant variations both in microstructure and mechanical properties, particularly influenced by carbon content and temperature reached. To replicate the effects of shoe braking, three different heat treatment conditions at various holding temperatures were applied to the samples. Ferritic-pearlitic steels exhibited properties primarily governed by the pearlite phase, impacting fracture toughness. Alloy-enriched steels displayed microstructures featuring traces of bainite, affecting mechanical properties. The heat treatment conducted at temperatures ranging from 700°C to 970°C resulted in substantial microstructural transformations, influencing mechanical properties. While some steels demonstrated improvements in mechanical properties post-treatment, most of them exhibited decreased performances. Notably, the heat treatment induced alterations in the original perlite morphology and grain size leading to a decrease in hardness and strength, coupled with an increase in ductility. However, fatigue crack growth behaviour remained consistent across materials, indicating minimal sensitivity to heat treatment. These findings offer valuable insights into railway wheel steel behaviour under thermal stress, informing strategies for enhancing performance and durability in real-world applications.

Keywords: Railway wheels, material testing, mechanical properties, thermal loading, shoe braking, fatigue behaviour.

1 Introduction

Railway wheel durability and performance are profoundly influenced by microstructural changes occurring in their surface layer during service, particularly under the thermal loading induced by shoe braking. This research delves into the relationship between microstructure and mechanical properties of railway wheels, due to various steel compositions, subjected to the heating from brake shoes. The impetus for this investigation stems from concerns raised by rolling stock suppliers regarding the spread of shoe braking, especially considering their application in high-speed train operations in order to reduce weights [1,2].

The study considers various scenarios, including emergency braking at speeds lower than 120 km/h [3], commonly employed in metro, suburban, and freight train operations. In particular, drag braking in freight transportation along slopes is a condition which applies very severe thermal loading to the wheel tread, whereas shoe braking in metro trains is characterized by frequent stop-and-go operations. Notably, the thermal cycle experienced by wheel treads, alternating between heating due to friction with the brake shoe and cooling from rail contact, poses significant challenges to the material integrity. This cyclic loading can induce high tensile stresses, microstructural modifications such as pearlite spheroidization or the formation of white etching layers, roughness by wear mechanisms on the tread and undesired tread profiles due to wear [4–14].

The consequences of manifesting high roughness and undesired tread profiles can potentially culminate in crack nucleation and propagation [12,15,16] Such cracks, exacerbated by rolling contact fatigue and external factors like fluid presence, can ultimately lead to wheel failure and derailment, highlighting the criticality of understanding material behaviour under thermal loading.

While significant strides have been made in elucidating microstructural changes under thermal exposure, comprehensive investigations into their influence on mechanical properties, especially for commonly used steels like ER7 and CLASS C, remain incomplete. This study bridges this gap by correlating microstructural observations with mechanical property assessments, employing standardized testing protocols and by taking into account the results of previous works carried out by the authors [3,17] together with new experimental data.

In light of escalating safety concerns within the railway industry, particularly regarding wheel fatigue and fracture resistance, this research assumes paramount importance. By scrutinizing the response of wheel materials to medium and high-temperature exposures, particularly from shoe braking, this study aims to inform the design and selection of materials, ensuring adherence to stringent safety Standards like the AAR M107/M208 and UIC 812.3. Ultimately, this endeavour strives to enhance rail and train safety on a global scale, safeguarding against catastrophic accidents stemming from wheel failure.

2 Materials and experimental procedures

2.1 Materials and heat treatments

This study originates from a comprehensive review of previous [3,17] research works, with the addition of new experimental data, aimed at comparing the overall effects of different steel chemical compositions utilized in railway applications, particularly focusing on their performance under shoe braking conditions. An investigation into eight distinct monobloc wheel steels is conducted encompassing variations in carbon (from 0.49% to 0.7%) and manganese (from 0.63% to 0.92%) content, with some steels having also a high silicon content (0.88% – 0.90%). The effects of silicon and manganese as alloying elements on steel properties are well-documented in literature [4–13]. Manganese enhances hardness, wear resistance, yield strength, and toughness, while also improving work-hardening behaviour [6–11]. Silicon improves hardness, wear resistance, and cyclic yield strength, and it delays pearlite spheroidization during annealing [4,6,11,12]. Both elements stabilize pearlite at high temperatures, reducing thermal sensitivity and mitigating thermal damage during braking. Manganese strengthens steel through solid solution strengthening and influences the formation and morphology of pearlite. Experimental studies have shown that reducing the distance between pearlite lamellae through controlled cooling rates enhances steel strength by limiting dislocation movement within the material, reducing the steel thermal sensitivity [5,11,13] thus alleviating the thermal damage due to braking.

Each steel grade is selected to represent a wide range of compositions commonly encountered in railway applications. These steels, namely ER7 (EN 13262), HYPERLOS®, ER8 (EN 13262), SUPERLOS®, ER-TEN, Class B (AAR M107/M208), SANDLOS®, and Class C (AAR M107/M208), underwent meticulous characterization to understand their response to heat treatment and their suitability for various operational conditions in railway environments. ER7 steel, compliant with the UIC 812.3 Standard, stands as one of the two approved steels for shoe braked wheels in Europe, catering to both freight cars and passenger transportation. Similarly, ER8 steel exhibits analogous compliance with stringent industry standards, offering a robust combination of strength and toughness necessary for demanding railway applications. HYPERLOS® steel, having an enhanced analytical calibration compared to ER7 steel, achieves superior mechanical properties through specialized heat treatment methods, resulting in a predominantly pearlitic microstructure and higher fracture toughness values [3]. SUPERLOS®, renowned for its silicon and manganese carbon composition, presents a unique pearlitic microstructure, providing exceptional wear and RCF resistance [18,19] garnering approvals from esteemed railway Standards such as BS 5892-3:1992+A2:2009 and EN 13262 as ERS8. In North America, CLASS B and CLASS C steels, mandated by the AAR M107/M208 Standard, find widespread usage in freight cars and locomotives, catering to varying service needs ranging from high-speed applications to heavy braking conditions. ER-TEN steel, derived from CLASS B AAR and J.Q3S/J.Q3R JIS steels, delivers heightened wear and RCF resistance due to its prevalently pearlitic microstructure. SANDLOS®, an upgraded material modified from CLASS B, presents elevated levels of manganese and silicon, further enhancing its mechanical properties and suitability

for extreme railway operations [20–22]. Chemical analysis obtained with the optical emission spectrometer ARL iSpark 8860, according to the ASTM E415 Standard for each steel is reported in Table 1.

Each steel underwent rim chilling, a heat treatment carried out during the wheel production, which entailed the austenitization of the wheel at 850°C followed by rapid cooling using water jets to achieve a fine pearlitic microstructure in the rim, mitigating detrimental phases like bainite. In addition, circumferential compressive residual stresses which originate in the rim during this heat treatment hinder the growth of RCF and thermal cracks. The subsequent tempering at 500°C and air-cooling further contributes to achieving the appropriate levels of hardness and toughness required to meet the mechanical property limits of the steel grade. This will be considered as the "as supplied" condition in this study.

Steel	C [%]	Si [%]	Mn [%]	S [%]	P [%]
ER7	0.49	0.34	0.75	0.002	0.008
HYPERLOS®	0.51	0.38	0.78	0.002	0.015
ER8	0.55	0.37	0.75	0.001	0.009
SUPERLOS®	0.52	0.90	0.92	0.002	0.013
ER-TEN	0.64	0.23	0.74	0.001	0.007
Class B	0.65	0.26	0.63	0.001	0.012
SANDLOS®	0.63	0.88	0.84	0.001	0.009
Class C	0.74	0.34	0.80	0.001	0.006

Table 1: Chemical compositions of the wheel steels in weight percent

Samples appropriately extracted from the wheel rim were then heat treated at various temperatures to simulate microstructural changes induced by shoe braking. The specimens were heated to the desired temperature at a rate of 40°C/h, held for 45 minutes, and air-cooled to achieve uniform microstructure. The holding time was determined by the UIC 510-5 Standard's fixed braking duration of 45 minutes. The holding temperature was chosen in accordance with the results of previous works [3,17], in which the authors estimate the temperature distribution in the rim section during tread braking using a Finite Element analysis. Temperature ranges were defined to investigate thermal effects in the wheel rim [6], with representative holding temperatures of 700°C, 750°C, and 970°C chosen for heat treatments to replicate shoe-braked wheel microstructures [3,17].

2.2 Experimental procedures

The experimental procedures undertaken in this study, better explained in previous works by the authors [3,17], aimed to comprehensively evaluate the mechanical properties and fracture behaviour of various wheel steels under different conditions, such as "as supplied" and heat-treated. The evaluation process involved several standardized tests and analytical techniques to ensure accuracy and reliability in the assessment.

Firstly, Brinell hardness tests were performed in accordance with the EN 13262 and AAR M-107/M-208 Standards. These tests were critical for evaluating the hardness distribution within the wheel rim, especially affected by rim chilling. Measurements were strategically taken at different depths within the rim, including points C (5 mm depth), points B (35 mm depth), and the transition between the rim and the web (point A). Standardized parameters such as a 5 mm diameter ball, an applied load of 7355 N, and a dwell time of 15 seconds were utilized. This detailed procedure ensured precise assessment of the hardness essential for wheel performance and durability.

Next, tensile tests were performed with cylindrical samples, measuring 10 mm in diameter and 50 mm in gauge length, extracted from the wheel rim at a depth of 15 mm below the running surface, as specified by the EN 13262 Standard. The tests were conducted at room temperature using an MTS servo-hydraulic testing machine, with a crosshead speed of 1 mm/min, as per the UNI EN 6892-1 Standard.

The experimental procedures also involved fracture toughness tests, in accordance with the EN 13262 and AAR M-107/M-208 Standards. For ER7 steel, EN 13262 Standard mandates a minimum toughness requirement to prevent undesired brittle fractures and ensure safety during service, while the AAR M-107/M-208 Standard does not specify fracture toughness requirements for CLASS B and CLASS C wheels. The fracture toughness tests were conducted following the ASTM E399 Standard using an MTS servo-hydraulic machine. Compact Tension samples with a thickness of 30 mm and width of 60 mm, denoted as CT30 specimens, were machined from the wheel rim. Notably, these dimensions represent the maximum allowed by the rim geometry. Six samples were extracted from each wheel in the untreated condition, spaced at 60-degree intervals along the tangential direction, to assess material uniformity across the wheel circumference. Additionally, three samples were extracted at positions 120 degrees apart from each other for each heat-treated condition. The load applied to the samples during the tests was aligned with the direction of tensile stresses experienced by the wheel rim in service, while the crack plane matched the orientation observed in service. Chevron notched samples were pre-cracked to an a/W ratio of 0.5 mm using the MTS system, with specific parameters including a frequency of 30 Hz, stress R-ratio of 0.1, and a final ΔK of 25 MPa$\sqrt{m}$. Crack Opening Displacement (COD) was measured using clip gauges to estimate the Load Line Displacement (LLD). The toughness parameter obtained under certain conditions was the apparent toughness parameter K_Q instead of fracture toughness K_{IC}. K_Q depends on the dimensions and geometry of the specimen, therefore it is not a characteristic of the material. However, with the same test piece and sampling position, it can be used to measure the fracture toughness of a wheel with that particular thickness. At the end of the test, the specimen was cut along the mid-plane orthogonal to the fracture surface and prepared for microstructural analysis, including grinding, polishing, and etching with 2 pct Nital to observe the steel microstructure and estimate the pearlite colony size number G (ASTM E 112) using an optical microscope.

The fatigue crack growth tests, conducted in compliance with ASTM E647 Standard, involved both as supplied and heat-treated specimens. CT25 samples, with thickness of 25 mm and width of 50 mm, were extracted from the wheel rim similarly

to CT30 specimens. These samples were pre-cracked to a initial crack length of 16 mm under load control. Testing was performed at room temperature using an MTS machine at 10 Hz with a sinusoidal wave and constant load ratio of 0.1. The crack propagation threshold ΔK_{th} was determined to be approximately 10^{-10} m/cycle. The experimental propagation curves were analyzed using the Paris model to derive material constants C_0 and n, essential for predicting crack growth behavior under varied loading conditions.

3 Results and discussion

3.1 As supplied condition

The investigation conducted on the steel samples "as supplied" provided many insights into their composition, microstructure, and mechanical properties, with significant implications for their performance in various railway applications. Table 2 provides a detailed overview of the microstructural constituents present in the examined steels, highlighting the prevalence of lamellar perlite, proeutectoid ferrite at grain boundaries, and, in certain cases (ER7, HYPERLOS®, SANDLOS® and Class C), traces of bainite, according to the cooling rates and CCT. As well known, variations in carbon content among the steels play a pivotal role in shaping their microstructure, as well as in the variation of mechanical properties [23].

The mechanical properties of ferritic-pearlitic steels are primarily governed by the pearlitic phase, which plays a key role in determining hardness and strength, while the presence of ferrite primarily influences ductility and toughness. Moreover, an increase in the proportion of pro-eutectoid ferrite tends to raise the critical cleavage fracture stress, as indicated by [24–26], which states that this stress is proportional to the cubic root of the proeutectoid ferrite fraction.

For instance, ER7 and HYPERLOS® steels, characterized by the lowest carbon content among the investigated grades, exhibited a higher fraction of ferrite, thus exhibiting lower hardness and strength, along with higher toughness than the other steels in the as supplied condition. On the other hand, Class C steel, with a carbon content close to the eutectoid composition, predominantly comprised perlite, thus exhibiting higher hardness and tensile strength with a lower toughness. Additionally, steels like SUPERLOS® and SANDLOS®, enriched with alloying elements such as silicon, displayed microstructures featuring traces of bainite, owing to modified CCT curves favouring bainite formation during heat treatment cooling.

The mechanical properties of the steels, including yield strength (YS), ultimate tensile strength (UTS), elongation (A%), reduction in area (Z%), fracture toughness (K_Q), and Brinell hardness (HB), were substantially influenced by both their chemical composition and microstructure. For instance, the Brinell hardness values presented in Table 3 varied significantly among the examined steels, confirming that as the carbon content in the steel composition increases, the Brinell hardness value also increases. As stated before, Class C steel exhibit the highest hardness attributed to its chemical composition close to the eutectoid composition, which favoured perlite formation, along with the presence of traces of bainite, a very hard structural constituent. Conversely, ER7 steel, characterized by lower carbon content,

demonstrated lower hardness due to the prevalence of softer proeutectoid ferrite. The influence of silicon in composition is clearly evident when comparing grades like SUPERLOS® and SANDLOS® to ER8 and Class B, respectively. Despite having similar compositions, the former two steels exhibit significantly higher silicon content, resulting in noticeably higher hardness compared to their counterparts [27–29]. Observations can be drawn regarding the hardness measurements obtained from the wheel rim across all steels. As illustrated in Table 3, there is a consistent decrease in hardness with increasing depth (from points C to A). This phenomenon can be attributed to the rim chilling heat treatment, a specialized hardening process designed to selectively harden the tread and flange of the rim.

The same principle as for hardness applies to other mechanical properties, as depicted in Table 4, and conversely, to the fracture toughness reported in Table 5: a higher carbon content increases mechanical properties and decreases fracture toughness, and vice versa. The yield strength, tensile strength, ductility and toughness obtained for CLASS B steel are similar to those found by Soares et al. [30]. Analogously, these mechanical properties are consistent with literature values even for CLASS C steel [31,32], and for ER7 and ER8 [5]. Figure 1a shows the apparent fracture toughness value (K_Q) of steels as supplied, correlates with their yield strength (YS) confirming the well-established and previously mentioned inverse proportionality between these properties.

Moreover, the fatigue crack growth behaviour of the steels, as detailed in Table 5, displayed remarkable similarities despite variations in chemical composition and microstructure. These similarities can be interpreted based on studies conducted by Liu et al. [33], who investigated the fatigue behaviour of six steels used in railway wheel production by Chinese state railways with carbon content ranging from 0.51% to 0.68%. The results indicated that the fatigue behaviour of the steels was not significantly affected by their chemical composition and microstructure. Other experimental studies have delved into the effect of the microstructure of ferritic-pearlitic steels, such as those used in monobloc railway wheel production, on their resistance to fatigue crack propagation. Korda et al. [34] highlighted that the resistance to fatigue crack propagation in steels with ferritic-pearlitic microstructure is significantly higher for those characterized by dispersed pearlitic phase, frequently interrupted by the presence of ferrite, compared to those with more interconnected pearlitic phase. This observation stems from the fact that within a microstructure characterized by the presence of different phases in contact with each other, the crack path becomes more tortuous and subject to frequent arrests. In confirmation, Guan et al. [35] found that in steels with ferritic-pearlitic microstructure containing traces of bainite, the latter either block the growth of fatigue crack or deflect its trajectory. However, Kròlicka et al. [36] reached opposite conclusions, comparing pearlitic and bainitic rail steel grades: by comparing the growth of a fatigue crack within a steel with pearlitic microstructure and one with bainitic microstructure, it emerged that despite the marked microstructural differences, the growth occurred in a very similar manner within the two steels.

In real-world wheel applications, increased friction and wear at the contact surface can lead to changes in steel properties due to high plastic strain, known as ratcheting. This affects fracture toughness and crack propagation rates. However, these changes

are limited to a surface layer, while severe damage occurs deeper within the wheel. Thus, alterations from ratcheting primarily impact initial crack propagation stages, which are less significant when assessing severe fatigue damage.

3.2 Heat-treated condition

The examination of the heat-treated samples reveals the impact of thermal stress from shoe braking on the microstructure and mechanical characteristics of the wheels. Detailed test results are provided in Tables 2, 3, 4, and 5. Figures 1, 2, and 3 summarize the percentage change in yield strength (YS), ultimate tensile strength (UTS), fracture toughness (K_Q) and propagation threshold (ΔK_{th}) values for steels based on the holding temperature reached during heat treatment, as well as a confrontation of the relationship between K_Q and YS of the steels after various heat treatment conditions.

Initially, all steels exhibit reduced hardness, yield strength, and tensile strength, along with increased ductility under heat-treated conditions compared to the as supplied condition. Moreover, these properties generally improve with increasing holding temperature during heat treatment, ranging from 750°C to 970°C, while ductility decreases. Notably, the holding temperatures exceed that of tempering after rim chilling (500°C), the final heat treatment in wheel production, indicating anticipated alterations in steel microstructure and mechanical properties. Given that the holding temperatures of the heat treatments fall within different regions of the iron-carbon phase diagram, various effects on the steels were anticipated. Consequently, the discussion of experimental outcomes is conducted separately for each heat treatment.

The heat treatment conducted at 700°C involves heating the steels just below the eutectoid temperature A_1 in the iron-carbon phase diagram. Microstructural changes show prevalently the formation of globular pearlite. This finding aligns with the discovery by Nikas et al. [5] that the process of pearlite spheroidization becomes noticeable at 450°C in ER8 wheel steel, a temperature significantly lower than the eutectoid temperature. Spheroidized pearlite is frequently seen close to the tread surface of wheels following use, as documented by Orringer et al. [11] and Cvetkovski et al. [6]. As shown in Table 2, the heat treatment induces alterations in the original perlite morphology, resulting in larger grain sizes compared to as supplied steels. The spheroidization of cementite lamellae within pearlite and the transformation of lamellar perlite contribute to a decrease in hardness and strength, coupled with an increase in ductility. Among the investigated steels, Class C demonstrates the greatest reductions in hardness and yield strength compared to the as supplied condition, highlighting its susceptibility to softening from spheroidization. Zucarelli et al. [32] also noted a reduction in the yield strength of Class C steel from room temperature to 500°C. This heat treatment results in a decrease in Brinell hardness at Point C for all examined steels, as indicated in Table 3. The reduction in hardness is attributed to grain size enlargement and the partial conversion of lamellar perlite into globular perlite, which is notably softer. However, Class C and SANDLOS® grades still exhibit the highest Brinell hardness values at Point C, respectively 245 ± 3 HB and 236 ± 5 HB, owing to their high carbon content and the presence of traces of bainite in their

microstructure. Conversely, ER8 steel demonstrates the lowest Brinell hardness at Point C after the 700°C treatment, at 201 ± 4 HB, due to the significant presence of pro-eutectoid ferrite in its microstructure. Table 4 presents the yield strength (YS) and ultimate tensile strength (UTS), along with percentage elongation (A%) and percentage reduction in area (Z%), of the steels under different heat treatment temperatures. Figure 2 illustrates the percentage variations in yield strength and ultimate tensile strength relative to values in the as supplied condition, with all steels showing a decrease in these properties after the 700°C treatment. This decrease can be attributed to the transformation of lamellar perlite into globular perlite and grain growth, phenomena common to all steels studied. SANDLOS® steel exhibits lower reductions in hardness and strength compared to the as supplied condition than CLASS B steel, attributed to higher Si content stabilizing pearlite at high temperatures. This stabilization decreases thermal sensitivity and alleviates thermal damage from braking. The toughness of SANDLOS® and CLASS B steels improves due to the spheroidization phenomenon, while ER7 steel shows a slight decrease in toughness. Toughness and tensile strength of ER7 steel after the 700°C heat treatment are partially consistent with previous results [37], where spheroidal particles positively influence toughness while drastically reducing strength.

The heat treatment carried out at 750°C involves heating the steels between A_1 and A_3 of the iron-iron carbide phase diagram, resulting in partial austenitization. Despite the higher holding temperature, the microstructural constituents and grain size are comparable to those observed after treatment at 700°C. Tensile property values for the investigated steels remain largely consistent with those treated at 700°C, with SUPERLOS® steel displaying the least degradation due to delayed spheroidization of perlite, attributed to the high Si and Mn content. Class C and SANDLOS® steels maintain high mechanical properties, while ER-TEN steel exhibits notable resistance, as its chemical composition promotes the formation of a microstructure rich in lamellar perlite even if after the heat treatment process it shows some traces of globular pearlite. However, Class C and ER-TEN steels experience significant decreases in tensile properties post-treatment at 750°C, albeit less than those observed at 700°C. ER7 steel demonstrates the lowest tensile properties after treatment at 750°C, influenced by larger grain size and lower carbon content favouring the formation of proeutectoid ferrite. Additionally, hardness values at Point C and fracture toughness parameters remain similar to those observed after treatment at 700°C. Class C steel maintains the highest hardness at Point C, while HYPERLOS® steel exhibits superior fracture toughness. The heat treatment at 750°C results in a mixed microstructure with varying ferrite phase fractions, negatively impacting steel toughness, particularly for ER7 steel due to its pronounced ferrite phase influence. Conversely, the effect on fracture toughness is minimal for CLASS B and SANDLOS® steels due to lower ferrite phase fractions.

The heat treatment conducted at 970°C involves subjecting the steels to temperatures exceeding the critical A_3 point, resulting in complete austenitization. Upon subsequent cooling, which occurs at a slower rate than the rapid cooling experienced during railway wheel rim chilling, all steels exhibit a notable increase in grain size compared to their original untreated state. This change in grain size, combined with alterations of the microstructure, significantly impacts the tensile

properties, Brinell hardness at Point C, and fracture toughness of the steels. The microstructure observed in steels treated at 970°C predominantly comprises lamellar perlite and proeutectoid ferrite, with occasional traces of globular pearlite, bainite or martensite. Despite the larger grain size post-treatment, the reduction in tensile properties compared to the untreated state is relatively less pronounced than that observed at lower treatment temperatures (700°C and 750°C). As for previous observations, Class C and SANDLOS® steels prove to be those with higher mechanical properties following treatment at 970°C, owing to their chemical composition rich in elements such as carbon (C), and, for the latter, silicon (Si). Cookson et al. [38] have highlighted that silicon and manganese delay the formation of perlite from the austenitic structure by slowing down the diffusion of carbon in iron necessary for the formation of ferrite and cementite lamellae, resulting in perlite forming at a lower temperature. Consequently, pearlite is characterized by a smaller interlamellar distance, which is the basis of the materials' higher tensile properties. Conversely, lower carbon steels display diminished tensile properties due to their larger grain size and increased presence of proeutectoid ferrite. Furthermore, the Brinell hardness at Point C exhibits a corresponding trend with the observed variations in tensile properties, with Class C and SANDLOS® steels consistently displaying higher hardness compared other steels. However, despite the improvements in certain mechanical properties, some steels experience a decrease in fracture toughness following treatment at 970°C, except for higher carbon steel (like ER-TEN, Class B, SANDLOS® and Class C) which shows similar if not slightly better toughness levels to their as supplied state. This reduction in toughness, particularly evident in lower carbon steels, can be attributed to microstructural changes induced by the heat treatment process. This phenomenon is also depicted in Figure 1b, where it can be observed that after the treatment at 970°C, the slope of the relationship between K_Q and YS changes significantly, tending to favour steels with higher yield strength. This contrasts with the treatments at 700°C and 750°C, which showed a slope similar to the results in the as-supplied condition, albeit shifted to the left.

Table 5 provides a comparison of subcritical crack propagation parameters across different heat treatment conditions for the steels. The parameters C_0, n, and ΔK_{th} exhibit consistent trends regardless of the treatment, with C_0 generally decreasing and n showing an opposite trend with increasing treatment temperature. This indicates a shift in crack propagation behavior, initially slowing down at lower stress intensity levels and then accelerating as the stress intensity approaches fracture values. ΔK_{th} tends to peak after treatment at 970°C, while most steels exhibit its minimum value in the as-supplied state, suggesting a significant increase in the threshold ΔK_{th} for crack propagation with higher treatment temperatures. Notably, HYPERLOS® steel shows minimal change post-treatment, with ΔK_{th} even lower than in the as supplied condition, highlighting its exceptional thermal performance. Fatigue crack growth tests depicted in Table 5 reveal consistent crack growth behaviour across all materials, indicating minimal sensitivity to heat treatment. This stability suggests that the materials' crack growth properties remain unaffected by thermal alterations, ensuring reliable performance even under severe thermal loading such as shoe braking.

Steel	Heat treatment condition	Microstructure	Grain Size Number G
ER7	As supplied	P + F +B	8
	700 °C	P + Pg + F	7.5
	750 °C	P + Pg + F + B	7.5
	970 °C	P + F	5 to 7.5
HYPERLOS®	As supplied	P + F + B	8.5
	700 °C	Pg + F + B	8.5
	750 °C	P + Pg + F + B	11.5
	970 °C	P + F + B	5
ER8	As supplied	P + F	7.5
	700 °C	Pg + F	7
	750 °C	P + Pg + F	8.5
	970 °C	P + Pg + F	4.5
SUPERLOS®	As supplied	P + F	7
	700 °C	P + Pg + F	7
	750 °C	P + Pg + F	9
	970 °C	P + Pg + F	4
ER-TEN	As supplied	P + F	6
	700 °C	P + F	5
	750 °C	P + Pg + F	6.5
	970 °C	P + Pg + F	3.5
Class B	As supplied	P + F	7.5
	700 °C	P + Pg + F	7
	750 °C	P + Pg + F	7
	970 °C	P + F	6.5
SANDLOS®	As supplied	P + F + B	8.5
	700 °C	P + Pg + F + B	7.5
	750 °C	P + Pg + F + B	7.5
	970 °C	P + F + B + M	6.5
Class C	As supplied	P + F + B	8
	700 °C	P + Pg + F + B	7.5
	750 °C	P + Pg + F	7.5
	970 °C	P + F + B + M	7
P pearlite, *Pg* globular pearlite, *F* ferrite, *B* bainite (traces), *M* martensite (traces).			

Table 2: Microstructure and grain size number G of the steels as supplied and under heat-treated conditions.

Steel	Heat treatment condition	HB Point A	HB Point B	HB Point C
ER7	As supplied	226	258 ± 4	273 ± 1
	700 °C	186	201 ± 1	208 ± 1
	750 °C	177	190 ± 2	199 ± 8
	970 °C	225	229 ± 3	231 ± 3
HYPERLOS®	As supplied	229	256	278
	700 °C	185	198	202
	750 °C	205	202	204
	970 °C	223	226	232
ER8	As supplied	236	265 ± 7	283 ± 4
	700 °C	195	198 ± 3	201 ± 4
	750 °C	213	210 ± 2	213 ± 4
	970 °C	195	199 ± 5	201 ± 5
SUPERLOS®	As supplied	245	262 ± 4	288 ± 2
	700 °C	206	211 ± 1	215 ± 3
	750 °C	224	230 ± 1	235 ± 3
	970 °C	232	231 ± 2	243 ± 7
ER-TEN	As supplied	257	277 ± 4	292 ± 5
	700 °C	211	210 ± 3	215 ± 2
	750 °C	221	224 ± 5	227 ± 6
	970 °C	255	247 ± 9	253 ± 5
Class B	As supplied	255	290 ± 4	310 ± 1
	700 °C	200	209 ± 3	220 ± 2
	750 °C	208	202 ± 2	205 ± 1
	970 °C	220	231 ± 8	226 ± 6
SANDLOS®	As supplied	280	300 ± 4	320 ± 1
	700 °C	240	242 ± 4	236 ± 5
	750 °C	229	230 ± 4	235 ± 2
	970 °C	286	287 ± 5	287 ± 2
Class C	As supplied	285	340 ± 4	355 ± 1
	700 °C	240	246 ± 3	245 ± 3
	750 °C	231	261 ± 2	255 ± 4
	970 °C	316	326 ± 9	341 ± 6

Table 3: Brinell Hardness values of the steels as supplied and under heat-treated conditions.

Steel	Heat treatment condition	Yield strength YS (MPa)	Tensile strength UTS (MPa)	Elongation to fracture A (%)	Reduction of area Z (%)
ER7	As supplied	610	911	14	39
	700 °C	451	693	24	60
	750 °C	424	692	24	62
	970 °C	467	837	17	46
HYPERLOS®	As supplied	568	885	28	65
	700 °C	444	674	26	59
	750 °C	444	712	19	54
	970 °C	493	856	19	53
ER8	As supplied	596	956	17	38
	700 °C	407	730	26	63
	750 °C	413	743	23	53
	970 °C	430	827	18	41
SUPERLOS®	As supplied	615	958	21	44
	700 °C	435	723	27	59
	750 °C	464	812	23	55
	970 °C	482	896	17	42
ER-TEN	As supplied	706	1062	13	34
	700 °C	425	730	26	59
	750 °C	441	819	22	49
	970 °C	498	908	15	34
Class B	As supplied	659	1035	15	28
	700 °C	453	756	22	57
	750 °C	429	726	24	57
	970 °C	437	866	15	36
SANDLOS®	As supplied	687	1148	14	41
	700 °C	501	869	23	51
	750 °C	490	814	19	48
	970 °C	620	1049	18	37
Class C	As supplied	730	1140	15	28
	700 °C	516	911	19	43
	750 °C	474	858	21	35
	970 °C	674	1146	13	23

Table 4: Tensile properties of the steels as supplied and under heat-treated conditions.

Steel	Heat treatment condition	Apparent Toughness Parameter K_Q $\left[MPa\sqrt{m}\right]$	C_0 $\left[\frac{m^{1-0.5n}MPa^{-n}}{cycles}\right]$	n	ΔK_{th} $\left[MPa\sqrt{m}\right]$
ER7	As supplied	89 ± 6	1.8×10^{-9}	3.3	7.4
	700 °C	75 ± 1	1.2×10^{-9}	4.2	8.5
	750 °C	72 ± 3	1.3×10^{-9}	3.4	8.4
	970 °C	66 ± 11	1.9×10^{-9}	3.3	7.8
HYPERLOS®	As supplied	102 ± 14	1.6×10^{-10}	3.3	8.1
	700 °C	103 ± 4	1.8×10^{-10}	3.3	7.9
	750 °C	99 ± 1	1.6×10^{-10}	3.4	8.5
	970 °C	63 ± 4	5.1×10^{-10}	2.9	7.3
ER8	As supplied	81 ± 5	3.8×10^{-9}	3.0	7.9
	700 °C	65 ± 8	1.6×10^{-10}	4.1	8.7
	750 °C	71 ± 2	7.7×10^{-10}	3.6	8.2
	970 °C	64 ± 8	7.1×10^{-10}	3.6	8.4
SUPERLOS®	As supplied	76 ± 4	2.3×10^{-9}	3.2	8.5
	700 °C	73 ± 3	8.3×10^{-10}	3.5	9.3
	750 °C	81 ± 1	7.7×10^{-10}	3.6	9.0
	970 °C	62 ± 4	2.6×10^{-10}	3.8	9.9
ER-TEN	As supplied	58 ± 5	2.8×10^{-9}	3.1	7.8
	700 °C	54 ± 4	6.0×10^{-10}	3.6	8.7
	750 °C	74 ± 5	6.6×10^{-10}	3.7	8.2
	970 °C	67 ± 4	1.3×10^{-10}	4.0	9.1
Class B	As supplied	58 ± 7	5.6×10^{-9}	3.0	7.1
	700 °C	64 ± 4	6.0×10^{-10}	3.6	8.6
	750 °C	65 ± 12	5.8×10^{-10}	3.7	9.2
	970 °C	60 ± 6	9.2×10^{-10}	3.6	7.7
SANDLOS®	As supplied	49 ± 3	8.6×10^{-9}	2.9	7.5
	700 °C	54 ± 5	5.3×10^{-10}	3.7	8.5
	750 °C	59 ± 5	2.2×10^{-9}	3.3	9.0
	970 °C	50 ± 6	1.2×10^{-9}	3.5	9.0
Class C	As supplied	48 ± 4	1.8×10^{-9}	3.4	7.2
	700 °C	47 ± 2	5.0×10^{-10}	3.7	9.4
	750 °C	48 ± 2	1.8×10^{-10}	4.0	10.1
	970 °C	49 ± 1	2.9×10^{-9}	3.2	9.4

Table 5: Apparent toughness parameter and fatigue crack growth test parameters of the tested steels as supplied and under heat-treated conditions.

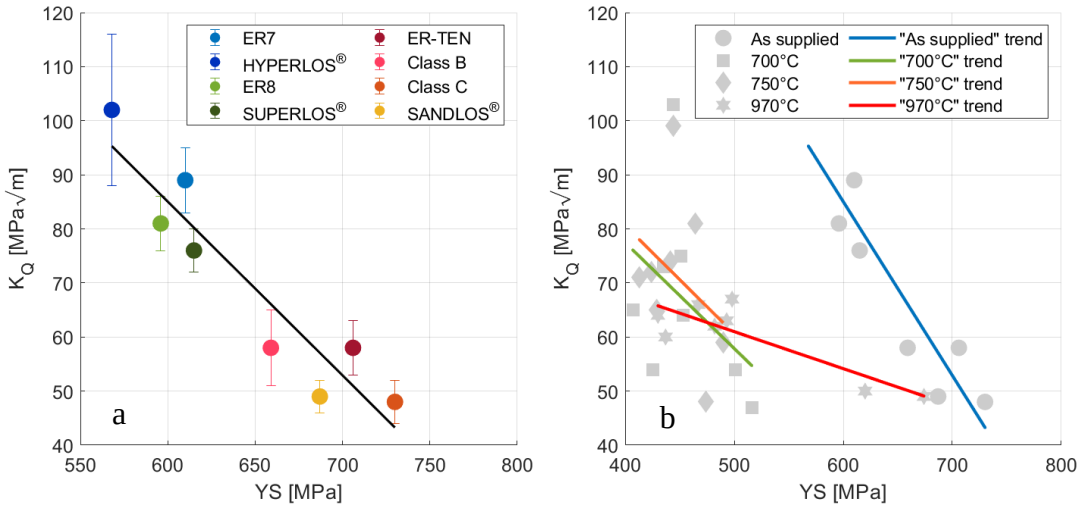

Figure 1: Apparent Toughness Parameter K_Q vs Yield Strength of the steels as supplied (a) and under different heat treatment conditions (b).

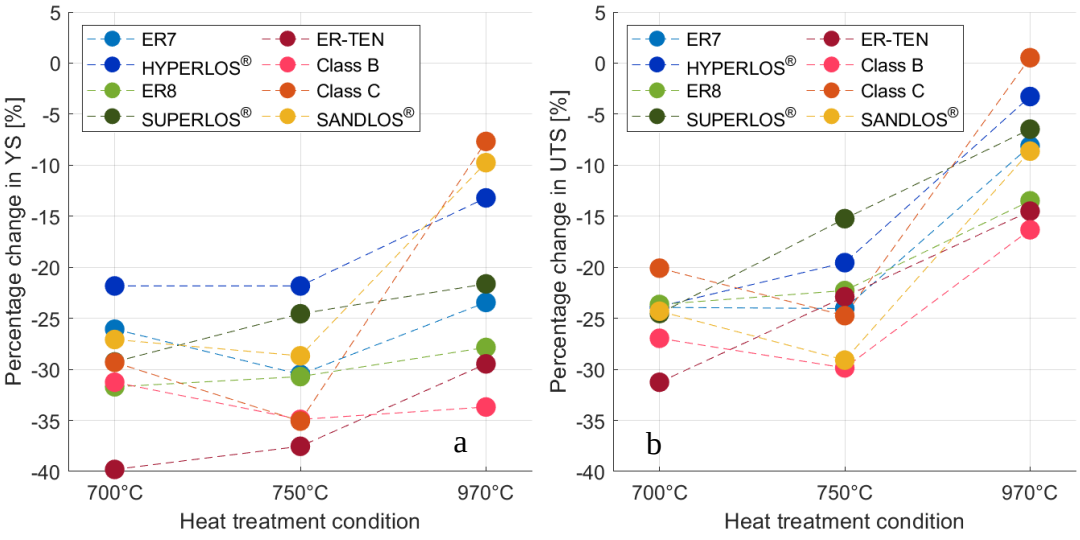

Figure 2: Percentage change in yield strength (a) and ultimate tensile strength (b) for steels based on the holding temperature reached during the heat treatment.

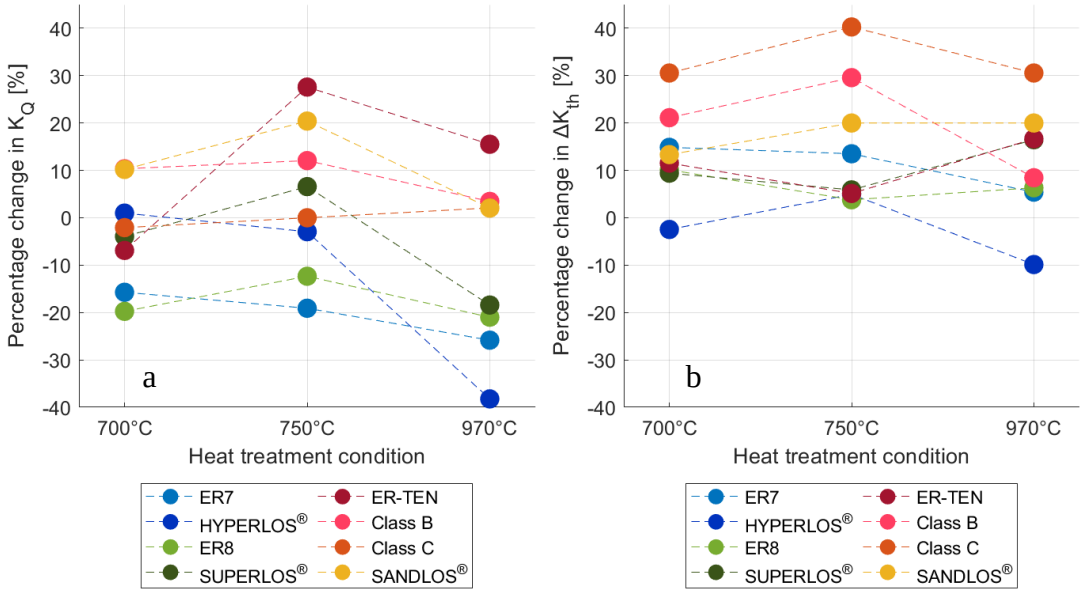

Figure 3: Percentage change in apparent toughness parameter K_Q (a) and threshold value of ΔK_{th}(b) for steels based on the holding temperature reached during the heat treatment.

4 Conclusions

The comprehensive investigation of eight distinct wheel steels in both as supplied and heat-treated conditions provides valuable insights into the effects of thermal stress from shoe braking on the microstructure and mechanical characteristics of railway wheels. The detailed test results presented highlight significant changes observed in steel properties under various heat treatment conditions. Initially, examination of the as supplied samples reveals distinct microstructures and mechanical properties among the investigated steels. Steels with varying carbon content exhibit different microstructures, influencing hardness, yield strength, and tensile strength. Notably, the mechanical properties of ferritic-pearlitic steels are primarily governed by the pearlite phase, with an increase in pro-eutectoid ferrite fraction influencing fracture toughness. For instance, ER7 steel, characterized by the lowest carbon content, exhibits higher ductility and toughness but lower hardness, strength, and yield strength compared to other steels. Conversely, Class C steel, with a carbon content close to the eutectoid composition, displays higher hardness and tensile strength but lower toughness due to predominant perlite composition. Additionally, steels enriched with alloying elements such as silicon exhibit microstructures featuring traces of bainite, influencing their mechanical properties. Upon heat treatment at holding temperatures ranging from 700°C to 970°C, steels undergo significant microstructural transformations, leading to alterations in mechanical properties. At 700°C, the formation of pearlite + globular pearlite + ferrite, with sometimes traces of bainite, is observed, resulting in reduced hardness and strength but increased ductility compared to untreated steels. Treatment at 750°C yields comparable microstructural constituents to those observed at 700°C, with relatively consistent tensile property values across

steels. However, ER7 steel exhibits notable decreases in mechanical properties due to its pronounced ferrite phase influence. At 970°C, complete austenitization of the microstructure occurs, resulting in significant grain growth and alterations in mechanical properties. Despite some improvements in mechanical properties for certain high carbon steels, such as ER-TEN, Class B, SANDLOS®, and Class C, others experience decreased fracture toughness. Among all steels, HYPERLOS® has shown the least reduction in mechanical properties even after post-treatment, resulting in being the most stable for applications at high temperatures; it only exhibits a significantly negative impact on fracture toughness after a very severe heat treatment at 970°C. However, overall, fatigue crack growth behaviour remains consistent across all materials, indicating minimal sensitivity to heat treatment. These findings provide valuable insights into the behaviour of railway wheel steels under thermal stress, informing potential strategies for enhancing their performance and durability in real-world applications.

Acknowledgements

This study was funded by Lucchini RS. The authors would like to thank Michele Nodari, Ivan Meloni, and the staff of the Metallurgy Department for their support.

References

[1] A. Mazzù, L. Provezza, N. Zani, C. Petrogalli, A. Ghidini, M. Faccoli, "Effect of shoe braking on wear and fatigue damage of various railway wheel steels for high speed applications", Wear 434–435 (2019) 203005. https://doi.org/10.1016/J.WEAR.2019.203005.

[2] M. Faccoli, L. Provezza, C. Petrogalli, A. Ghidini, A. Mazzù, "A Small-Scale Experimental Study of the Damage Due to Intermittent Shoe Braking on the Tread of High-Speed Train Wheels", Tribology Transactions 63 (2020) 1041–1050. https://doi.org/10.1080/10402004.2020.1787568.

[3] M. Faccoli, A. Ghidini, A. Mazzù, "Experimental and Numerical Investigation of the Thermal Effects on Railway Wheels for Shoe-Braked High-Speed Train Applications", Metallurgical and Materials Transactions A 49 (2018) 4544–4554. https://doi.org/10.1007/s11661-018-4749-2.

[4] G.J. Moyar, D.H. Stone, "An analysis of the thermal contributions to railway wheel shelling", Wear 144 (1991) 117–138. https://doi.org/10.1016/0043-1648(91)90010-R.

[5] D. Nikas, J. Ahlström, A. Malakizadi, "Mechanical properties and fatigue behaviour of railway wheel steels as influenced by mechanical and thermal loadings", Wear 366–367 (2016) 407–415. https://doi.org/10.1016/J.WEAR.2016.04.009.

[6] K. Cvetkovski, J. Ahlström, B. Karlsson, "Thermal degradation of pearlitic steels: influence on mechanical properties including fatigue behaviour",

Materials Science and Technology 27 (2011) 648–654. https://doi.org/10.1179/026708310X520538.
[7] J. Ahlström, B. Karlsson, "Microstructural evaluation and interpretation of the mechanically and thermally affected zone under railway wheel flats", Wear 232 (1999) 1–14. https://doi.org/10.1016/S0043-1648(99)00166-0.
[8] J. Ahlström, B. Karlsson, "Analytical 1D model for analysis of the thermally affected zone formed during railway wheel skid", Wear 232 (1999) 15–24. https://doi.org/10.1016/S0043-1648(99)00167-2.
[9] J. Jergéus, "Martensite formation and residual stresses around railway wheel flats", Proc Inst Mech Eng C J Mech Eng Sci 212 (1998) 69–79. https://doi.org/10.1243/0954406981521051.
[10] K. Handa, Y. Kimura, Y. Mishima, "Surface cracks initiation on carbon steel railway wheels under concurrent load of continuous rolling contact and cyclic frictional heat", Wear 268 (2010) 50–58. https://doi.org/10.1016/J.WEAR.2009.06.029.
[11] O. Orringer, D.E. Gray, "Thermal cracking in railroad vehicle wheels subjected to high performance stop braking", Theoretical and Applied Fracture Mechanics 23 (1995) 55–65. https://doi.org/10.1016/0167-8442(95)00004-X.
[12] M. Petersson, T. Vernersson, "Noise-related roughness on tread braked railway wheels-experimental measurements and numerical simulations", Wear 253 (2002) 301–307. https://doi.org/10.1016/S0043-1648(02)00121-7.
[13] L. Ghidini, M. Faccoli, N. Zani, C. Petrogalli, S. Bonometti, A. Mazzu, "An innovative small-scale testing procedure to study damage in shoe-braked wheels", Proc Inst Mech Eng F J Rail Rapid Transit (2023). https://doi.org/10.1177/09544097231173738.
[14] L. Ghidini, A. Mazzù, S. Bonometti, M. Faccoli, "Study of the thermo-mechanical damage in steels for shoe-braked railway wheels using innovative small-scale tests | Studio del danneggiamento termomeccanico di acciai per ruote ferroviarie frenate a ceppi mediante test innovativi small-scale", Ingegneria Ferroviaria 78 (2023) 547–559. https://doi.org/10.57597/IF.0708.2023.ART.1.
[15] T. Vernersson, "Thermally induced roughness of tread-braked railway wheels: Part 1: brake rig experiments", Wear 236 (1999) 96–105. https://doi.org/10.1016/S0043-1648(99)00260-4.
[16] T. Vernersson, "Thermally induced roughness of tread braked railway wheels: Part 2: modelling and field measurements", Wear 236 (1999) 106–116. https://doi.org/10.1016/S0043-1648(99)00261-6.
[17] M. Faccoli, A. Ghidini, A. Mazzù, "Changes in the Microstructure and Mechanical Properties of Railway Wheel Steels as a Result of the Thermal Load Caused by Shoe Braking", Metallurgical and Materials Transactions A 50 (2019) 1701–1714. https://doi.org/10.1007/s11661-019-05135-x.
[18] A. Ghidini, M. Diener, A. Gianni, J. Schneider, SUPERLOS ®: Innovative Steel by Lucchini RS For High-speed Wheel Application, Lucchini RS, 2012. https://lucchinirs.com/expertise/books/ (accessed March 8, 2024).

[19] A. Mazzù, C. Petrogalli, M. Lancini, A. Ghidini, M. Faccoli, "Effect of Wear on Surface Crack Propagation in Rail–Wheel Wet Contact", J Mater Eng Perform 27 (2018) 630–639. https://doi.org/10.1007/s11665-018-3185-1.
[20] A. Ghidini, M. Faccoli, A. Mazzù, C. Petrogalli, "An innovative steel grade family for forged-rolled solid wheels designed for sandy environments", Ing. Ferrov 73 (2018) 729–742.
[21] M. Faccoli, C. Petrogalli, M. Lancini, A. Ghidini, A. Mazzù, "Effect of desert sand on wear and rolling contact fatigue behaviour of various railway wheel steels", Wear 396–397 (2018) 146–161. https://doi.org/10.1016/J.WEAR.2017.05.012.
[22] M. Faccoli, C. Petrogalli, A. Ghidini, "On Mechanical Properties of New Railway Wheel Steels for Desert Environments and Sand Caused Wheel Damage Mechanisms", J Mater Eng Perform 28 (2019) 2946–2953. https://doi.org/10.1007/s11665-019-04049-4.
[23] A. Calik, A. Duzgun, O. Sahin, N. Ucar, "Effect of Carbon Content on the Mechanical Properties of Medium Carbon Steels", 65 (2010) 468–472. https://doi.org/doi:10.1515/zna-2010-0512.
[24] J.F. Knott, Fundamentals of Fracture Mechanics, Butterworth, 1973. https://books.google.it/books?id=gXtWq1_eHC8C.
[25] Y.J. Park, I.M. Bernstein, "The process of crack initiation and effective grain size for cleavage fracture in pearlitic eutectoid steel", Metallurgical Transactions A 10 (1979) 1653–1664. https://doi.org/10.1007/BF02811698.
[26] A. Hohenwarter, A. Taylor, R. Stock, R. Pippan, "Effect of Large Shear Deformations on the Fracture Behavior of a Fully Pearlitic Steel", Metallurgical and Materials Transactions A 42 (2011) 1609–1618. https://doi.org/10.1007/s11661-010-0541-7.
[27] T. Gladman, P. FB, "Some aspects of the structure-property relationships in high-carbon ferrite-pearlite steels", (1972).
[28] D. Zeng, L. Lu, N. Zhang, Y. Gong, J. Zhang, "Effect of different strengthening methods on rolling/sliding wear of ferrite–pearlite steel", Wear 358–359 (2016) 62–71. https://doi.org/10.1016/J.WEAR.2016.04.003.
[29] D. Zeng, L. Lu, Y. Gong, Y. Zhang, J. Zhang, "Influence of solid solution strengthening on spalling behavior of railway wheel steel", Wear 372–373 (2017) 158–168. https://doi.org/10.1016/J.WEAR.2016.12.025.
[30] H. Soares, T. Zucarelli, M. Vieira, M. Freitas, L. Reis, "Experimental characterization of the mechanical properties of railway wheels manufactured using class B material", Procedia Structural Integrity 1 (2016) 265–272. https://doi.org/10.1016/J.PROSTR.2016.02.036.
[31] T. Kato, Y. Yamamoto, H. Kato, S. Dedmon, J. Pilch, "Effect of fracture toughness on vertical split rim failure in railway wheels", Eng Fract Mech 186 (2017) 255–267. https://doi.org/10.1016/J.ENGFRACMECH.2017.09.025.
[32] T. Zucarelli, L. Moreira Filho, H. Soares, M. Vieira, L. Reis, "Experimental characterization of the mechanical properties of railway wheels manufactured using class C material", Theoretical and Applied Fracture Mechanics 85 (2016) 134–139.

[33] Z.X. Liu, H.C. Gu, "Failure modes and materials performance of railway wheels", J Mater Eng Perform 9 (2000) 580–584. https://doi.org/10.1361/105994900770345728.
[34] A.A. Korda, Y. Miyashita, Y. Mutoh, T. Sadasue, "Fatigue crack growth behavior in ferritic–pearlitic steels with networked and distributed pearlite structures", Int J Fatigue 29 (2007) 1140–1148. https://doi.org/10.1016/J.IJFATIGUE.2006.09.008.
[35] M. Guan, H. Yu, "In-situ investigation on the fatigue crack propagation behavior in ferrite-pearlite and dual-phase ferrite-bainite low carbon steels", Sci China Technol Sci 56 (2013) 71–79. https://doi.org/10.1007/s11431-012-5047-7.
[36] A. Królicka, G. Lesiuk, K. Radwański, R. Kuziak, A. Janik, R. Mech, T. Zygmunt, "Comparison of fatigue crack growth rate: Pearlitic rail versus bainitic rail", Int J Fatigue 149 (2021) 106280. https://doi.org/10.1016/J.IJFATIGUE.2021.106280.
[37] M. Diener, A. Ghidini, "Fracture Toughness: A Quality Index for Railway Solid Wheels", Mater Perform Charact 3 (2014) 286–304. https://doi.org/10.1520/MPC20130047.
[38] J. Cookson, P. Mutton, Performance of wheels in heavy haul service: matching microstructures to service conditions, in: CORE 2014, Rail Transport for a Vital Economy, Conference on Railway Excellence, Adelaide, South Australia, 2014.